

# Measurement of relative isotopic yield distribution of even-even fission fragments from $^{235}\text{U}(n_{th},f)$ following $\gamma$ ray spectroscopy

Aniruddha Dey,<sup>1,2,\*</sup> D.C. Biswas,<sup>1,†</sup> A. Chakraborty,<sup>2</sup> S. Mukhopadhyay,<sup>1</sup>  
A. K. Mondal,<sup>2</sup> L. S. Danu,<sup>1</sup> B. Mukherjee,<sup>2</sup> S. Garg,<sup>3</sup> B. Maheshwari,<sup>4</sup>  
A. K. Jain,<sup>4</sup> A. Blanc,<sup>5</sup> G. de France,<sup>6</sup> M. Jentschel,<sup>5</sup> U. Köster,<sup>5</sup>  
S. Leoni,<sup>7</sup> P. Mutti,<sup>5</sup> G. Simpson,<sup>8</sup> T. Soldner,<sup>5</sup> C. A. Ur,<sup>9</sup> and W. Urban<sup>10</sup>

<sup>1</sup>*Nuclear Physics Division, Bhabha Atomic Research Centre, Mumbai 400 085, India*

<sup>2</sup>*Department of Physics, Siksha Bhavana, Visva-Bharati University,  
Santiniketan, West Bengal 731 235, India*

<sup>3</sup>*School of Physics and Astronomy,  
Shanghai Jiao Tong University, Shanghai 200240, P. R. China*

<sup>4</sup>*Amity Institute of Nuclear Science and Technology,  
Amity University UP, Noida 201 313, India*

<sup>5</sup>*Institut Laue-Langevin, 71 Avenue des Martyrs, 38042 Grenoble CEDEX 9, France*

<sup>6</sup>*GANIL, BP 55027, F-14076 Caen Cedex 5, France*

<sup>7</sup>*Università degli Studi di Milano, I-20133 Milano, Italy*

<sup>8</sup>*LPSC, 53 Avenue des Martyrs, 38026 Grenoble, France*

<sup>9</sup>*INFN Sezione di Padova, I-35131 Padova, Italy*

<sup>10</sup>*Faculty of Physics, University of Warsaw, PL 02-093 Warszawa, Poland*

(Dated: April 7, 2021)

## Abstract

A detailed investigation on the relative isotopic distributions has been carried out for the first time in case of even-even correlated fission fragments for the  $^{235}\text{U}(n_{th},f)$  fission reaction. High-statistics data were obtained in a prompt  $\gamma$  ray spectroscopy measurement during the EXILL campaign at ILL, Grenoble, France. The extensive off-line analysis of the coincidence data have been carried out using four different coincidence methods. Combining the results from 2-dimensional  $\gamma - \gamma$  and 3-dimensional  $\gamma - \gamma - \gamma$  coincidence analysis, a comprehensive picture of the relative isotopic yield distributions of the even-even neutron-rich fission fragments has emerged. The experimentally observed results have been substantiated by the theoretical calculations based on a novel approach of isospin conservation, and a reasonable agreement has been obtained. The calculations following the semi-empirical GEF model have also been carried out. The results from the GEF model calculations are found to be in fair agreement with the experimental results.

---

\* [deyaniruddha07@gmail.com](mailto:deyaniruddha07@gmail.com)

† [dcbiswas11@gmail.com](mailto:dcbiswas11@gmail.com)

## I. INTRODUCTION

Nuclear fission is an extremely complex phenomenon with the collective involvement and rearrangement of the participating nucleons in a multi-dimensional deformation space. In general, a nucleus splits into two fragments of comparable sizes during a fission process. The process is also involved with the emission of neutrons, gamma rays, and light charged particles, which carry the information of the dynamical evolution of the underlying fission dynamics. Fission also acts as a source of production for many rare isotopes, which can be harvested for use in fundamental research as well as applied areas like nuclear medicine and technology. The neutron-rich fission fragment nuclei that are produced in a fission process, display a remarkable range of exotic nuclear phenomena which are in general, investigated experimentally through in beam gamma-ray spectroscopic method.

Many scientific investigations have already been carried out on the fragment nuclei that are produced in  $^{252}\text{Cf}$  [1–6] and  $^{248}\text{Cm}$  spontaneous fissions (SF) [7–10], neutron induced fission [11–13], as well as multiple heavy- and light-ion induced fission reactions[14–18]. However, it is worth noting that the fission products are not the same in each fission reaction. Rather, each of them is produced in a certain percentage (characteristics of their fission “yield”) of the total number of fissions. As an example, the fission yields of the neutron-rich fragments in the mass  $A\approx 100$  region is significantly larger in the  $^{235}\text{U}(n_{th},f)$  fission reaction than those from the  $^{252}\text{Cf}$  and  $^{248}\text{Cm}$  SF reactions [19].

It is worthwhile mentioning that the isotopic yield distributions of a fission process carry valuable information about that particular fission process, and provide the necessary observables for making comparison with the predicted results from theoretical models of fission. Thus, it is of great importance to basic research as well as applications in reactor physics. For example, the knowledge of these yield distributions provides the key data to understand issues related to nuclear fuel waste. Fission yield data are also of importance in the various nuclear energy applications, such as, reactivity or decay heat in nuclear power plants, post-irradiation scenarios, neutron-flux determination, and so on.

There are several available techniques to estimate experimentally the relative isotopic yield distribution of fission fragments. In the case of  $^{235}\text{U}(n_{th},f)$  fission reaction, such studies have already been carried out using recoil mass separators, time-of-flight measurements using MWPCs (Multi Wire Proportional Counter) and radiochemical analysis [20–24]. It

is to be pointed out here that the majority of the previous investigations were aimed for extracting the yields of the isotopes belonging to the lighter fragment region. The necessary attempt for extracting the relative isotopic yields for the correlated fission fragments for  $^{235}\text{U}(n_{th},f)$  through the prompt  $\gamma$  ray spectroscopic method has not been undertaken prior to the present investigation. The only available isotopic yield data for this fissioning system based on gamma spectroscopy is from the work of Mukhopadhyay *et al.* [13]. The results obtained from this previous investigation were found to be very limited due to the use of a very small array comprising of only two Compton suppressed clover Ge detectors. In the present investigation, an attempt has been made to extract precisely the relative isotopic yield distribution of all the possible even-even fission fragment pairs populated within the sensitivity limit of the measurement. A large array of gamma detectors were used for the present investigation and both the  $\gamma - \gamma$  and  $\gamma - \gamma - \gamma$  coincidence data were used for extracting the yields. The advantage of triple gamma coincidence measurements is that they can provide sufficient resolving power to analyse the complex gamma radiation following fission. Identification of new transitions in a selected nucleus can be achieved by gating a known transitions in this nucleus and/or in the complementary fission fragment.

It is notable here that the prompt  $\gamma$ -ray spectroscopic method has got an added advantage over the other methods for measuring the isotopic yields. This is due to the fact that one can ideally measure the fragments with a unit mass resolution through the  $\gamma$  ray spectroscopic method. However, special care is to be taken for extracting unambiguous yields through the spectroscopic method. The factors that make this approach highly sensitive are (a) the lack of reasonably developed level schemes in the literature for certain neutron-rich fragment nuclei, (b) unavoidable yield contributions from the precursors' beta decay, (c) large electron conversion probability for certain  $\gamma$ -transitions, and (d) the presence of low spin milli-second and micro-second isomers *etc.*. In the present work, the uncertainties due to all the above mentioned factors have been thoroughly considered and the necessary corrections are taken into account within the limit of practical applicability.

The unambiguous results obtained from the present investigation have been compared with the results from a new type of calculations carried out under the novel formalism of isospin conservation (ISCF). The results from isospin conservation formalism, together with the semi-empirical GEneral description of Fission (GEF) model calculations [25], have been found to be in fair agreement with the experimental findings.

## II. EXPERIMENTAL SETUP

The experiment was performed at the PF1B neutron beam line of the high-flux reactor facility at the Institut Laue-Langevin (ILL), Grenoble, France. The fission fragments were produced following the induced fission of  $^{235}\text{U}$  by thermal neutrons and identified through standard  $\gamma$  ray spectroscopic method. The collimated neutron beam flux was  $\approx 10^8$  n.  $\text{s}^{-1}$   $\text{cm}^{-2}$  at the target position. The proper collimation of the neutron beam was made using a series of lithium and boron collimators mounted upstream from the target position. This collimated neutron beam was allowed to impinge upon a  $\text{UO}_2$  target of thickness  $\approx 600$   $\mu\text{g}/\text{cm}^2$ . The target was about 99.7% enriched in  $^{235}\text{U}$ . The target was sandwiched between thick backings in order to stop the fission fragment nuclei and avoid the Doppler shifts of the  $\gamma$  peaks. The gamma rays emitted from the various fission fragments were detected by the EXILL array [26]. The array was comprised of eight EXOGAM Clover detectors, six large coaxial detectors from GASP, and the two clovers from the ILL. The pictorial view of the experimental setup is shown in Fig. 1. The BGO anti-Compton shields were used as Compton suppressors for the EXOGAM and GASP detectors. The EXOGAM clovers were mounted in a  $90^\circ$  ring around the target position. The other detectors were placed in two other rings positioned at  $45^\circ$  and  $135^\circ$ . The total photo-peak efficiency for the array was estimated as about 6% [27]. The data were collected with a trigger-less, digital data acquisition system based on 14 bit 100 MHz CAEN digitizers. Details about the electronics and data acquisition systems can be found in Ref. [28]. A total of about  $2 \times 10^{10}$   $\gamma - \gamma$  and about  $3.5 \times 10^9$   $\gamma - \gamma - \gamma$  coincidence events were recorded during the experiment.

## III. DATA ANALYSIS AND EXPERIMENTAL RESULTS

The raw data files collected during the experiment were converted into structured ROOT tree files for an appropriate prompt coincidence time window of 200 ns. An in-house data sorting code was developed to read the ROOT tree files, apply quadratic calibration, generate spectra for each detector segment as well as for clovers in add-back mode. The spectra were generated in RADWARE [29] format. Subsequently  $\gamma - \gamma$  coincidence matrices, and  $\gamma - \gamma - \gamma$  cubes were constructed for further off-line analysis. The detailed off-line coincidence spectral analysis was performed using the standard analysis software packages, RADWARE

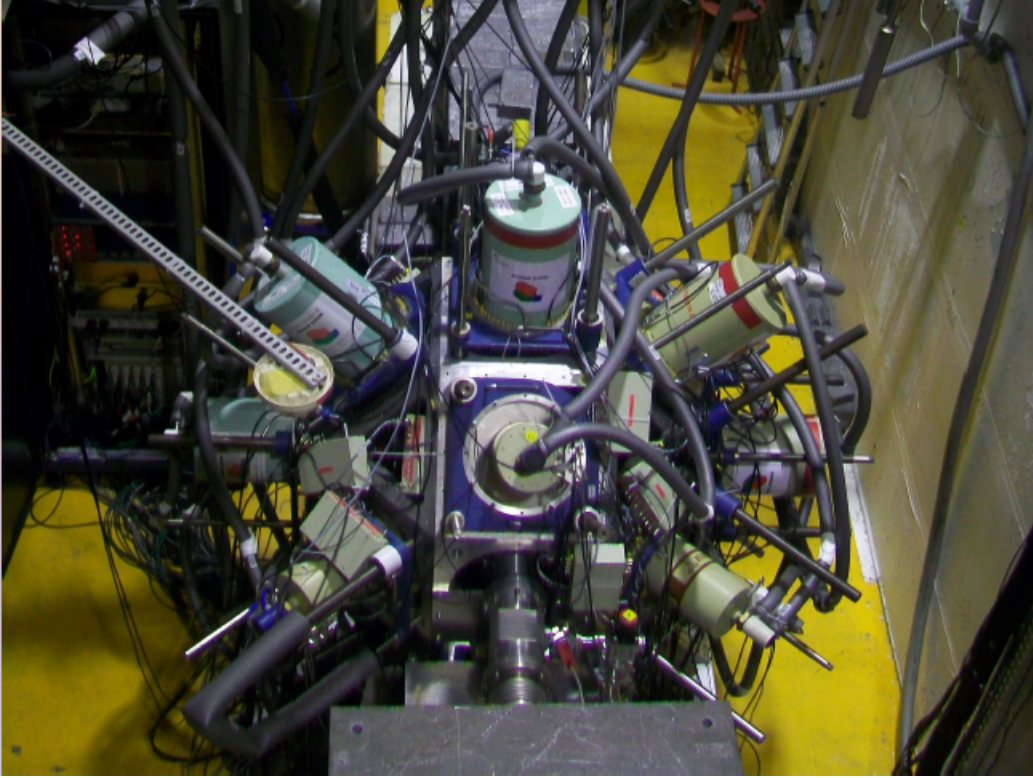


FIG. 1. (Color online) A top-view of the experimental EXILL setup at the PF1B neutron beam line area of the high-flux reactor facility at the Institut Laue-Langevin (ILL), Grenoble, France.

[29, 30] and Tv [31]. In the present work, the relative isotopic yield distributions of several complementary even- $Z$ , even- $N$  fission fragment pairs have been measured. The complementary fragment pairs that have been analyzed from the present set of data are (Mo-Sn), (Zr-Te), (Sr-Xe), (Kr-Ba), and (Se-Ce); thereby covering a mass range from 80 to 150. Based on the selection of gating and observed transitions, the yields of the complementary fragment pairs have been extracted by implementing four different methods of analysis. The execution of this exercise was needed to gather complete knowledge about the relative merits and demerits of each of the analysis method, which in turn was found to be very helpful in standardizing the best analysis procedure for extracting the relative isotopic yields of the complementary fission fragment pairs. The four different analysis methods have been described one by one in the follow up discussion. (a) Method-1: In this method, the yield of a particular fragment nucleus has been extracted from the area of the peak corresponding to its  $2_1^+ \rightarrow 0_1^+$  transition seen in the coincidence spectrum generated by setting the gate on the  $4_1^+ \rightarrow 2_1^+$  transition of the same nucleus.

(b) Method-2: In this particular method, the coincidence gates are set on the  $2_1^+ \rightarrow 0_1^+$  transitions of the two correlated fission fragment nuclei. The coincidence peak yields of the respective  $4_1^+ \rightarrow 2_1^+$  transitions of all the possible complementary fragments are then extracted simultaneously.

(c) Method-3: The peak yield of the  $2_1^+ \rightarrow 0_1^+$  transition of the fission fragment has been measured from the coincidence spectrum generated by setting the coincidence gates on  $4_1^+ \rightarrow 2_1^+$  and  $2_1^+ \rightarrow 0_1^+$  transitions belonging to all the other possible complementary fragments.

(d) Method-4: Any two of the  $2_1^+ \rightarrow 0_1^+$ ,  $4_1^+ \rightarrow 2_1^+$ , and  $6_1^+ \rightarrow 4_1^+$  transitions of a fragment nucleus have simultaneously been gated, and the resultant coincidence spectrum has been generated. The area of the peak corresponding to the third transition of the concerned nucleus has been fitted from the coincidence spectrum and the yield of the fragment has been extracted.

It is to be noted here that Method-1 deals with two-fold  $\gamma - \gamma$  coincidence analysis; whereas the rest of the three methods are based on the analysis using three-fold  $\gamma - \gamma - \gamma$  coincidence data. As an example, these methods have been applied to the (Zr-Te) complementary fragment pair. The partial level scheme showing the yrast-line transitions of  $^{100}\text{Zr}$  and  $^{134}\text{Te}$  are shown in Fig. 2. The representative coincidence spectra obtained under different analysis methods is shown in Fig. 3. The figure demonstrates that there is gradual improvement in the peak-to-total ratio for the concerned peaks obtained from Method-4, Method-1, Method-3, and Method-2, respectively. Here, the peak-to-total ratio parameter can be defined as the ratio between the area of a peak and the total area in a given spectrum.

In order to obtain unambiguous results for the isotopic yields of the complementary fission fragment pairs, a detailed analysis of the coincidence data has been carried out using the aforesaid four different methods. This exercise has helped us to gather knowledge about the relative merits and demerits of each of the analysis method which in turn was found to be very helpful in standardizing the best analysis procedure and obtaining comprehensive results. A detailed description on the merits and demerits for each of the above mentioned methods have been put forward in the follow up discussion.

Measurements of the relative isotopic yield distribution of fission fragments using prompt gamma ray spectroscopy have been carried out in most of the previous investigations following Method-1, which involves the analysis using two-fold  $\gamma - \gamma$  coincidence data. As

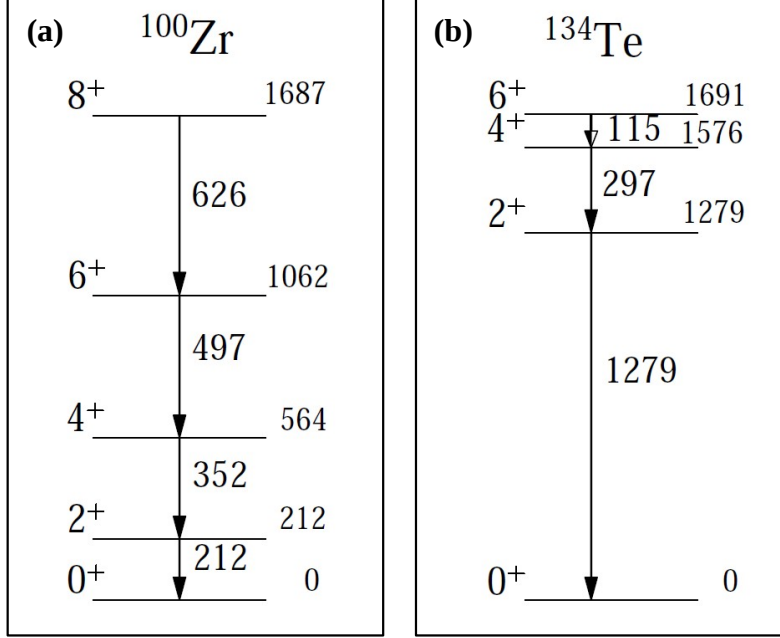


FIG. 2. (Color online) Partial level scheme of (a)  $^{100}\text{Zr}$  and (b)  $^{134}\text{Te}$ , respectively. All the relevant spectroscopic information have been taken from the ENSDF database [32].

mentioned in the aforesaid section, the present investigation has been carried out using a large array of gamma detectors. Hence, the off-line processing of data into three-fold  $\gamma-\gamma-\gamma$  coincidences with sufficient statistics could be possible. Such analysis processes ensure better selection and identification of the fragments so that the accurate extraction of the relative yields of the fission fragments could be possible. As noted above, apart from Method-1, all the other methods (Method-2, 3, and 4) are based on  $\gamma-\gamma-\gamma$  cube analysis. In the case of Method-4, there appears to be a serious limitation for extraction of the population yield of a fragment nucleus. This is due to the fact that in the case of a vibrational nucleus, the population strength for the states above the  $4_1^+$  level gets fragmented among the close-lying multi-phonon vibrational states. Hence, the strength of the  $6_1^+ \rightarrow 4_1^+$  transition does not simply reflect total yield at that particular excitation regime. Hence, this method looks to be only applicable in the case of fragments having rotational character. The fission fragments having both the low-lying rotational and vibrational structures are populated well in the present investigation. Hence, Method-4 does not seem to be the appropriate method for extracting the isotopic yields. Hence, the results obtained with this method are not reported in the present work.

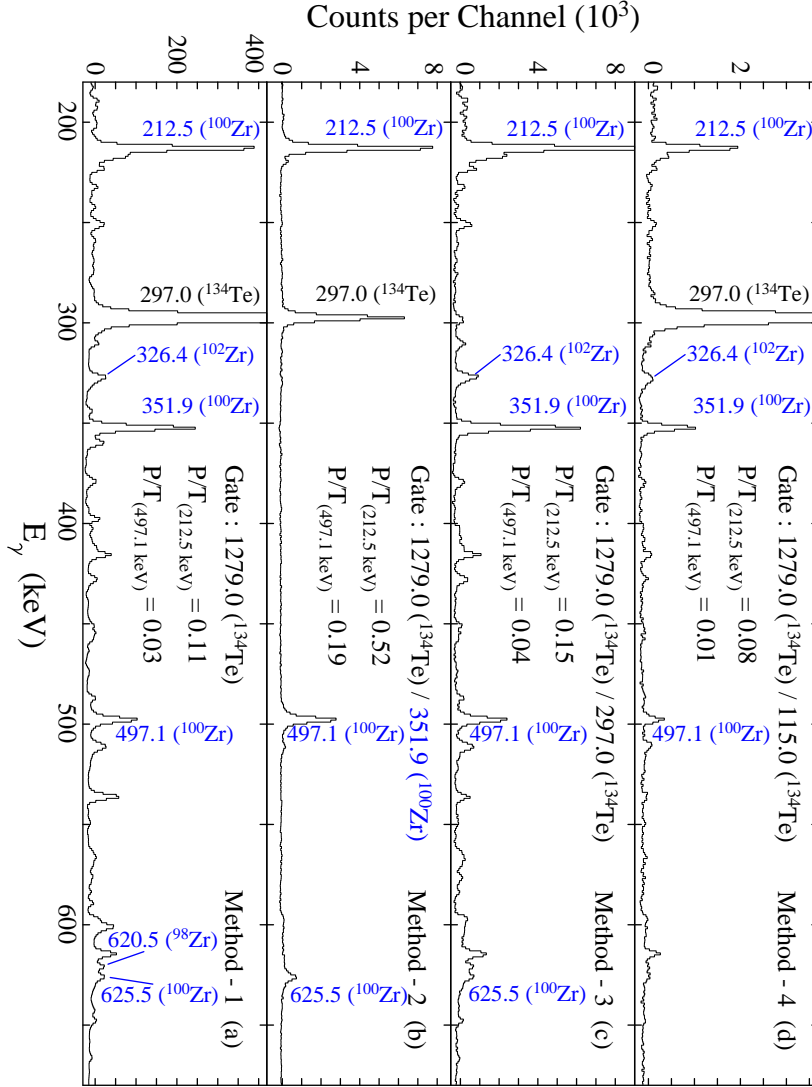


FIG. 3. (Color online) Representative coincidence spectra obtained by Method-1, Method-2, Method-3 and Method-4 are shown in panel (a), (b), (c) and (d) respectively. For panel (a), the gate is set on 1279.0( $2_1^+ \rightarrow 0_1^+$ )-keV transition of  $^{134}\text{Te}$ . For panel (b), the gates are set on 1279.0( $2_1^+ \rightarrow 0_1^+$ )-keV transition of  $^{134}\text{Te}$  and 351.9 ( $4_1^+ \rightarrow 2_1^+$ )-keV transition of  $^{100}\text{Zr}$ . For panel (c), the gates are set on 1279.0( $2_1^+ \rightarrow 0_1^+$ )- and 297.0( $4_1^+ \rightarrow 2_1^+$ )-keV transition of  $^{134}\text{Te}$ . For panel (d), the gates are set on 1279.0( $2_1^+ \rightarrow 0_1^+$ )- and 115.0( $6_1^+ \rightarrow 4_1^+$ )-keV transition of  $^{134}\text{Te}$ .

In a recent study for the spontaneous fission of  $^{252}\text{Cf}$  [33], Method-3 has been utilized for the whole set of analysis, and for the first time a second mode of fission has been reported. But since in this method both the gamma coincidence gates are set on one particular fragment, the observed coincidence population statistics for the complementary fragment nucleus is relatively lower in nature. This approach offers a very good scope of selectivity for the complementary fragments, but suffers from problems in extracting the yields for the probable isotopes having poor population strengths. In the present data set, the yields of the isotopes such as  $^{82}\text{Se}$ ,  $^{104}\text{Zr}$ ,  $^{98,100}\text{Mo}$ ,  $^{134}\text{Xe}$ , and  $^{144}\text{Ce}$  could not be measured due to the aforesaid limitation associated with Method-3. Method-2 involves the cross gating gamma transitions for selecting simultaneously both the complementary fragments. Hence, this method not only deals with the proper identification of the complementary fragments, but also provides better enhancement in statistics for the coincidence peaks corresponding to the concerned complementary fragments.

#### **A. Additional corrections associated with the determination of fragment yields**

In the present work, we have incorporated three different types of corrections for extracting unambiguously the relative isotopic yields of the complementary fission fragment pairs. These include the necessary corrections associated with (a) conversion electron process, (b) contribution from precursors' beta decay, and (c) presence of milli or micro second isomers. It is to be pointed out here that while dealing with Method-2 and -3, the correction factor for contribution from precursors' beta decay is not needed as both the complementary fission fragments are simultaneously observed in one step coincidence yield measurement. For the estimation of conversion electron probability, the BrIcc code [34] has been utilized for all the  $\gamma$ -transitions having energies below 500 keV. It is to be pointed out here that for proper estimation of the correction factor (required only for Method-1 and -4) associated with the contribution from the precursors' beta decay to the lower mass isotopes, the corresponding yields from Method-2 have been utilized. A comparison between the yield of a fragment nucleus measured from self-gating and that from the complementary fragment gating (all the even channels are taken into account) gives the excess contribution from the beta feeding. These correction factors are then utilized in both Method-1 and -4. This approach of correction has been made possible due to the availability of high statistics  $\gamma - \gamma - \gamma$

coincidence data. It is notable here that huge contributions (under Method-1 and -4) from the precursors' beta decay have been observed in the cases of  $^{100}\text{Mo}$ ,  $^{130}\text{Te}$ ,  $^{134}\text{Xe}$ , and  $^{144}\text{Ce}$ . The additional corrections to the yields were required due to the presence of low-spin  $\mu$ -second isomers in several fragment nuclei populated in the present work. These include the isomeric states belonging to  $^{126-132}\text{Sn}$ ,  $^{132}\text{Te}$ , and  $^{136}\text{Xe}$ . The necessary correction factor due to the presence of an isomer is calculated by estimating at first the yield of the particular fragment above this concerned isomeric state. Following this, the proper estimation for the proportionate decay based on the coincidence time window and the isomeric level life-time has been made. On comparing the coincidence yields of the  $2_1^+ \rightarrow 0_1^+$  transition extracted from the gates setting on the transitions lying above and below the particular isomeric state, the necessary correction factor is estimated subsequently. Apart from the above mentioned corrections, additional corrections due to the associated side-feedings have also been appropriately incorporated in the present work for all the four analysis procedures. The concerned side-feedings are due to those transitions which directly decay to the  $2_1^+$  level of a particular fission fragment. It is a matter of common fact that nuclei which have low-lying vibrational level structures are associated with comparably larger amount of side feeding contributions. In the present work, it has been observed that the transitions decaying from  $2_2^+$ ,  $3_1^-$ , and  $4_2^+$  levels are the dominant side-feeding contributors. The estimated side-feedings (in percentages) for different fission fragment nuclei are shown in Table II. While dealing with the extraction of isotopic yields of the complementary fission fragments, a significant amount of direct feeding of the gamma rays from the excited  $2_2^+$  levels to the ground states of the respective fragments have also been observed in a few cases. For  $^{88}\text{Se}$ ,  $^{90}\text{Kr}$ ,  $^{96}\text{Sr}$ , and  $^{98}\text{Zr}$ , the estimated feedings from such transitions are found to be (in percentage) 18, 16, 7, and 12, respectively. The direct feedings of  $E3$  transitions from the  $3_1^-$  level to the ground states have also been observed in a few cases. These include the fragments  $^{96}\text{Zr}$ ,  $^{132}\text{Sn}$ , and  $^{146}\text{Ba}$ . The concerned additional yields of these fragments due to  $E3$  feedings have been extracted from the known intensity ratios between the  $3_1^- \rightarrow 0_1^+$  and  $3_1^- \rightarrow 2_1^+$  transitions available from the ENSDF database [32].

## B. Observations and error analysis

For the majority of the fission fragment nuclei, it has been observed that the  $2_1^+ \rightarrow 0_1^+$  and  $4_1^+ \rightarrow 2_1^+$  transitions are nearly of equal intensity which suggests that the process of de-excitation occurs predominantly through this cascade. However, the major limitations for extracting the yields following gamma ray spectroscopic method arises from the non-availability of detailed level schemes for many of the neutron-rich nuclei. The limitations obviously seem to be more pronounced while dealing with  $\gamma - \gamma - \gamma$  coincidence analysis for the the non-yrast excited states. However, one can assume that contributions from any of the unobserved feeding transitions from the non-yrast states to the ground and  $2_1^+$  states would be very feeble. Hence the contributions from such unobserved feedings to the final yields of the fission fragments would be negligible.

The raw yield distributions of the complementary fission fragment pairs obtained from Method-1, Method-2, and Method-3 are shown respectively in Figs. 4 (a), (b), and (c). It is interesting to note that the yields for the Sn isotopes extracted from Method-1 are found to be significantly less than that of the complementary fragment pairs of Mo isotopes. The extracted results for the Mo-Sn complementary fragments from Method-2 do not indicate such an obvious difference in the yields while Method-3 shows an opposite behavior (i.e. yield of Sn isotopes are more than Mo isotopes). For the pair of Se-Ce also, this behavior of reversing the trend in yield has also been observed. These observations brings out the limitations in the analysis procedure of Method-1 as described in the aforesaid section. Similar type of anomalies in the measured yields for the pair of Mo-Sn isotopes has also previously been reported in the spectroscopic work of  $^{238}\text{U}(n,f)$  reaction [35], where the data were analyzed using Method-1. However, another group verified from direct fission fragment yield measurements that there was no significant yield difference for the Mo-Sn pair in  $^{238}\text{U}(n,f)$  reaction [36]. The observed anomaly in the present and previous spectroscopic measurements is related to the  $\gamma$ -multiplicity difference among the correlated fragment pairs of Mo-Sn. The results from the theoretical calculations of Ref.[37] also highlights this observation. In the present work, the uncertainties (about 3% has been considered) due to efficiency corrections of the  $\gamma$ -transitions have been added in quadrature to the statistical uncertainties to obtain the final uncertainties associated with the extracted yields of the fragments. The uncertainties due to the implementation of various corrections are also included in quoting the final

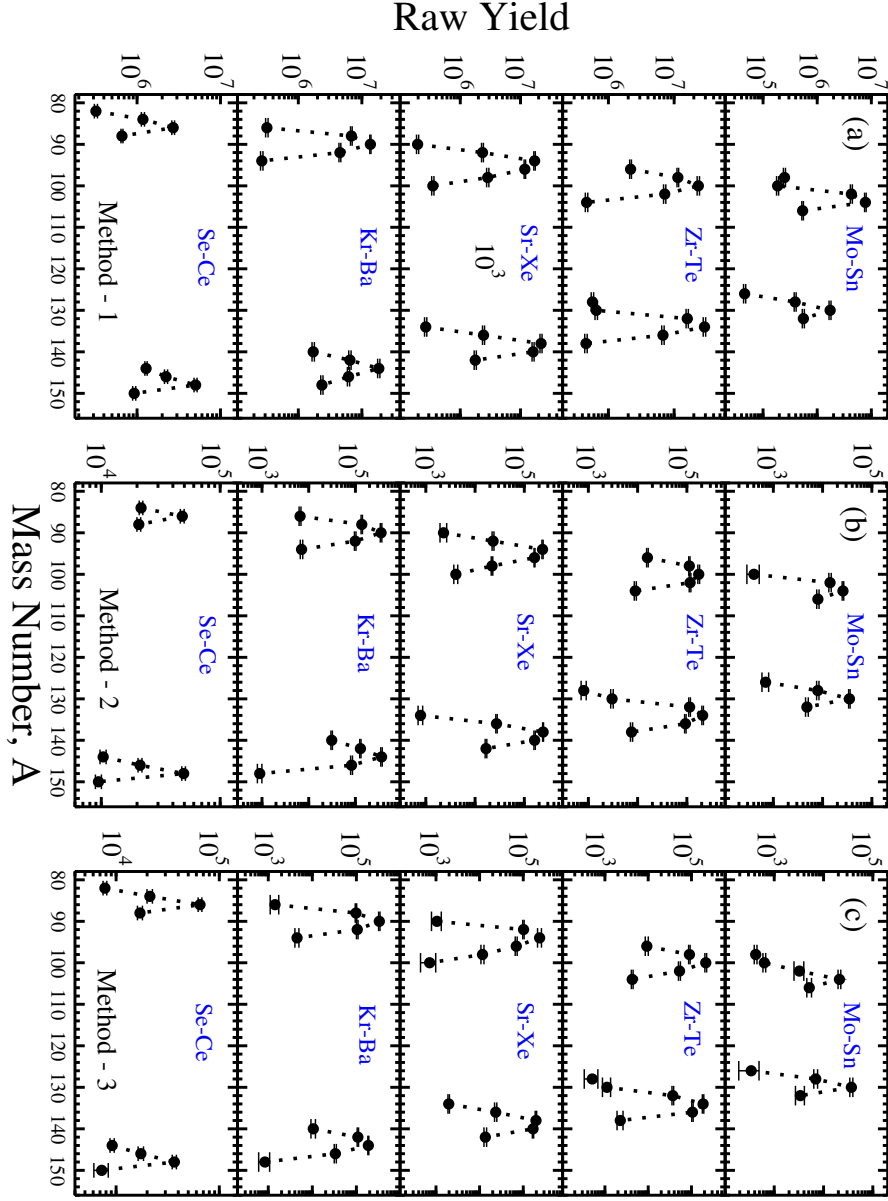


FIG. 4. (Color online) Raw isotopic yield distribution of the complementary even-even fission fragment pairs extracted from  $\gamma-\gamma$  coincidence analysis through (a) Method-1, (b) Method-2, and (c) Method-3. See text for details.

uncertainties associated with the measured yields of the fragments. The relative yields (in %) of the complementary fragments obtained from Method-1, -2, and -3 are compared in Fig. 5. The figure indicates marginal difference in yields of the complementary fragment

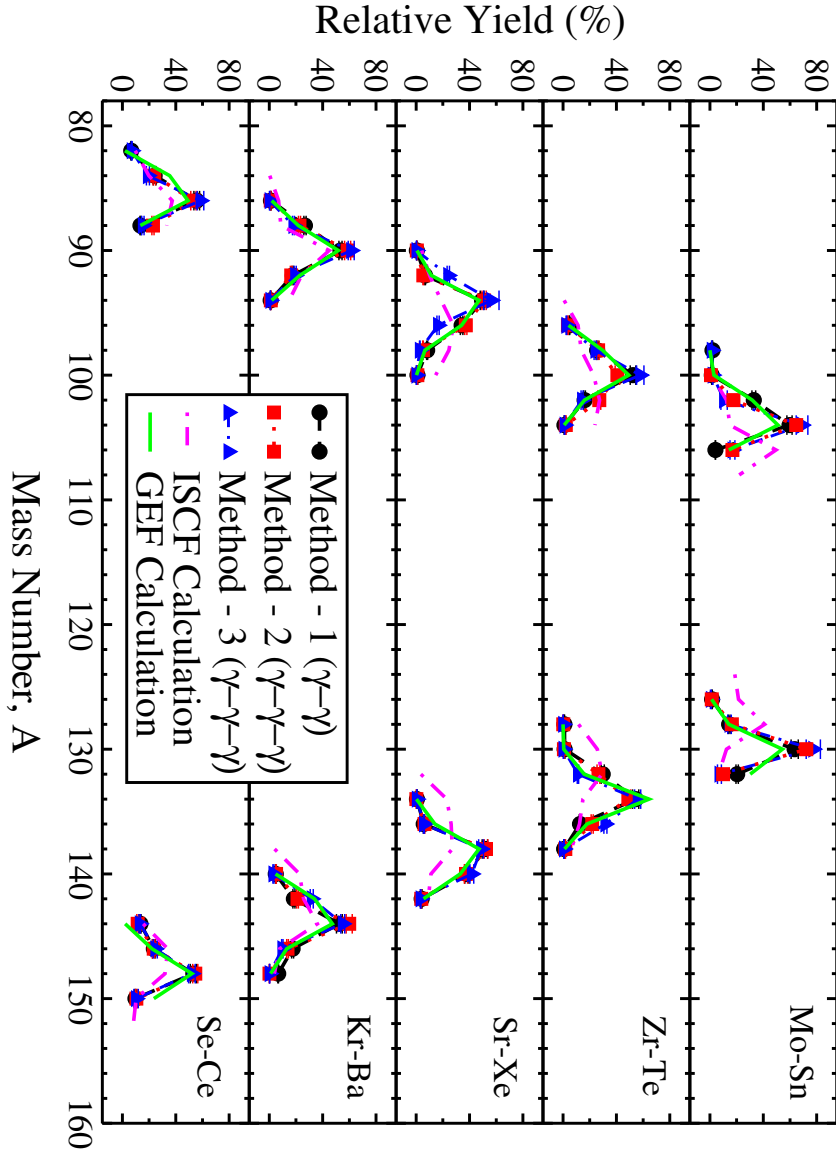


FIG. 5. (Color online) Comparison of relative yield distribution for the complementary even-even fission fragment pairs extracted from the analysis of Method-1, Method-2, and Method-3. The predicted results from GEF and ISCF calculations are also shown. The sum of the relative yields of all the isotopes of a particular fragment has been normalized to 100.

pairs for all the three methods. However, the raw data depicted in the Fig. 4 indicates that there are about 63%, 5% and 27% differences in the maximum yields of the complementary

fragment pair of Mo-Sn corresponding to Method-1, 2, and 3, respectively. These percentage values have been calculated using the ratio between the difference in the maximum peak yields of the pair of complementary fragments and their corresponding mean values.

The comparison of the extracted yields of the pairs of complementary fragments obtained from the present (following Method-2) and previous investigations is shown in Fig. 6. The previous two investigations were carried out by Lang *et al.* [21] and Strittmatter *et al.* [23] using the Lohengrin mass separator and HIAWATHA recoil mass spectrometer, respectively. For making a qualitative comparison between the extracted yields from the present measurement and the absolute yields from the previous measurements, the absolute yield data have been multiplied by a factor of 1000 and plotted accordingly in Fig. 6. As can be seen from the figure, the results from the previous investigations are available for the lighter fragments of each of the complementary pairs and the patterns of yield distribution appear to collate well with the results from the present investigation. The present work thus provides a complete landscape for the relative isotopic yield distribution pattern of each of the even-even fragment pairs, populated within the limit of measurable sensitivity of the present experimental set up, following  $^{235}\text{U}(n_{th},f)$  reaction. Thus, the experimental results from the present investigation seem to provide a better testing ground for comparing the results from the models developed under different formalism. The predicted results from different models have been compared with the results obtained from the present investigation in the follow up section. The yield data obtained from the present investigation has further been fitted using a double Gaussian function. The fitted yield curves of the different fragment pairs are also shown in Fig. 6. The yield data of a particular pair of complementary fragments has been fitted with the constraints that the area under both the Gaussian curves are kept fix while all the other parameters are kept free. The Gaussian parameters extracted from the fittings are enlisted in Table I. A mean value of dispersion parameter,  $\sigma_Z = 1.38$  has been obtained from the tabulated data. The values of the dispersion parameters obtained from the present work are found to be consistent with those obtained from the empirically developed  $A'_p$  model [38].

## IV. DISCUSSIONS

It is generally believed that the isospin remains a good quantum number in lighter nuclei having a few protons. With increasing proton numbers, the purity of isospin breaks down due to the emergence of strong Coulomb interactions. However, following theoretical calculations by Lane and Soper [39], it is highly interesting to note that the purity of isospin gets restored in heavy neutron-rich nuclei due to the presence of excess number of neutrons which would dilute the isospin impurity of the  $N = Z$  core of the heavy nucleus. Hence, the neutron rich nuclei produced through spontaneous fissions, heavy-ion induced fusion-fission and other induced-fission reactions should provide the necessary ground for testing the purity of isospin. Jain *et al.* [40] proposed the aforesaid idea, and developed the necessary formalism based on Kelson's arguments [41], for assigning the specific isospin to neutron-rich fragment nuclei produced in a fission process. Subsequent calculations for the relative yields of the fission fragments were carried out based on the assigned isospin and related algebra. The formalism has already been tested for the relative isotopic yields of the correlated even-even fission fragments produced through heavy-ion induced fusion-fission reactions and thermal neutron induced fission of  $^{245}\text{Cm}$  [42–44]. A very good agreement was obtained between the theoretical and the experimental relative yields for the correlated even-even fission fragment pairs. In the present work, the isospin conservation formalism has been adopted for new calculations on the even-even fission-fragment yields from the  $^{235}\text{U}(n_{th},f)$  reaction, and the results have been compared with those extracted from the high-statistics experimental data.

The values of the total isospin ( $T$ ) and the third component of isospin ( $T_3$ ) of all the even-even fragment nuclei that are possible in the  $^{235}\text{U}(n_{th},f)$  reaction have been uniquely assigned (following the prescription proposed by Jain and collaborators [42–44]), and are tabulated in Table III. A pictorial representation of the assigned values of  $T$  and  $T_3$  for different fragment nuclei is shown in Fig. 7. The assignment of the values is based on two conjectures proposed by Kelson [41]. These are: (a) the higher the number of neutrons ( $\nu$ ) emitted in a fission process, the greater is the probability for the formation of highly excited states with  $T > T_3$ , and (b) the fission fragment nuclei are preferably formed in isobaric analog states (IAS). It has already been explained that for the IAS, it is sufficient to consider three member isobaric multiplets (see Table III) for assigning a proper isospin value ( $T$ ) to the fragment nuclei of a particular mass number [43].

Considering only the isospin part of the total nuclear wave function, the yield of a particular pair of even-even fragment nuclei (represented as  $F_1$  and  $F_2$ ) produced via “ $\nu$ ” number of neutron emission channel is given as [44]:

$$I_\nu = \langle T_{F_1} T_{F_2} T_{3F_1} T_{3F_2} | T_{RCN} T_{3RCN} \rangle^2 = (CGC)^2 \quad (1)$$

where,  $RCN$  denotes the residual compound nucleus that has been formed after the emission of  $\nu$  number of neutrons from the initial compound nucleus ( $CN$ ) such that,  $RCN = F_1 + F_2$ , with  $T_{RCN} \geq T_{3RCN}$ ; the isospin and third component of isospin of  $RCN$  is represented by  $T_{RCN}$  and  $T_{3RCN}$ , respectively; the terms  $T_{F_1}$  ( $T_{3F_1}$ ) and  $T_{F_2}$  ( $T_{3F_2}$ ) denote the isospins (third components of isospins) for the fragments,  $F_1$  and  $F_2$ , respectively; the term on the right hand side of the above equation represents the square of the Clebsch Gordon Coefficients (CGC).

The calculated isotopic yields for the even-even complementary fission fragment nuclei are depicted along with the experimental results in Fig. 5. It is obvious from the figure that the calculated yields are in reasonable agreement with those extracted from the experimental data. This leads us to conclude that the isospin remains an approximately good quantum number for the neutron-rich fission fragments, produced in thermal neutron induced fission of  $^{235}\text{U}$ . It is worthwhile mentioning that the calculation using the isospin conservation formalism is valid for the compound nucleus (CN) based fissioning systems only. Further, the formalism assumes that all the neutrons from the compound nucleus are emitted in one single step, thereby making no distinction between the pre- and post-scission neutrons.

Further calculations were carried out under the framework of the semi-empirical GEF model[25]. The GEF model is based on a general approach to nuclear fission and provides a considerable insight into the physics of the fission process. Using the GEF model, most of the fission observables can be calculated with a precision that complies with the needs for applications in nuclear technology. The simulation code based on the GEF model is designed as a Monte-Carlo formalism that follows all the quantities of the fissioning systems with their correlations and dependencies. It is evident from Fig. 5 that the GEF model reproduces the experimentally deduced relative isotopic yield distributions of the correlated even-even fragment nuclei quite well.

Thus it can be summarized that the overall agreement between the calculated results from the semi-empirical based GEF model calculations and the experimental data is quite evident.

Moreover, it should be noted that the results from the standard GEF model calculations are found to be in reasonable agreement with those obtained from the new calculations based on isospin conservation formalism for the  $^{235}\text{U}(n_{th},f)$  reaction.

## V. CONCLUSION

Correlated neutron rich fission-fragment nuclei produced in the  $^{235}\text{U}(n_{th},f)$  reaction have been investigated following prompt high-resolution  $\gamma$  ray spectroscopy method. The high-statistics coincidence data were obtained during the EXILL campaign at ILL, Grenoble, France. The relative isotopic yield distributions of the even-even fission fragments have been extracted combining the results from  $\gamma-\gamma$  and  $\gamma-\gamma-\gamma$  coincidence analysis. The extraction of yields of the correlated fragment pairs have been carried out using four different methods of analysis. Merits and demerits of the methods have been discussed in detail. The best suitable method of analysis for the extraction of unambiguous yields of the correlated fragment pairs has been identified. An attempt has been made for interpreting the experimental results by a theoretical model calculation based on isospin conservation formalism (ISCF). However, only a reasonable agreement has been observed between the theoretical and experimental results presented in this paper, suggesting an improvement in the model is required to explain the fission yield distribution. The experimental results have also been compared with those obtained from the semi-empirical GEF model calculations. The predicted results from the two different theoretical approaches are found to be in reasonable agreement with each other.

## VI. ACKNOWLEDGMENTS

The authors are grateful to the EXOGAM collaboration for the loan of the detectors, to GANIL for providing assistance during installation and dismantling, and to the INFN Legnaro laboratory for the loan of the GASP detectors. Two of the authors (A.D. and A.C.) gratefully acknowledge the financial assistance received from the DAE-BRNS, Govt. of India (Project Sanction No.: 37(3)/14/17/2016-BRNS) for carrying out this work. One of the authors (A.K.J) acknowledges the support from Science and Engineering Research Board (Govt. of India) of a Grant No. CRG/2020/000770. One of the authors (S. Garg) acknowl-

TABLE I. The extracted Gaussian parameters obtained from the fitting of the relative isotopic yield distributions of the complementary fission fragment pairs of  $^{235}\text{U}(n_{th},f)$ .

Sl. No	Fission Fragment	Z	$\sigma_Z$	$A_P$	$N_P/Z$
1	Se	34	1.24	85.58	1.49
2	Kr	36	1.43	89.84	1.49
3	Sr	38	1.26	94.42	1.49
4	Zr	40	1.82	100.21	1.49
5	Mo	42	1.52	103.59	1.44
6	Sn	50	1.07	129.87	1.59
7	Te	52	1.56	133.74	1.56
8	Xe	54	1.44	138.61	1.55
9	Ba	56	1.27	143.92	1.55
10	Ce	58	1.22	147.79	1.54

edges the partial support by the National Natural Science Foundation of China (Grant No. U1932206) and by the National Key Program for S & T Research and Development (Grant No. 2016YFA0400501).

TABLE II: List of fission fragment nuclei having measurable amount of feeding from the different excited levels, other than that from the  $4_1^+$ , to the  $2_1^+$  level. The nuclei those have the feeding component from the  $4_1^+$  level only are not enlisted in the table. The measured feeding contributions (in %) from different components are shown in the rightmost column of the table. All the other relevant spectroscopic quantities in the table has been taken from the ENSDF database [32].

Nuclei	Ground state transitions (keV)	$J_i^\pi \rightarrow J_f^\pi$	Feeding transitions (keV)	$J_i^\pi \rightarrow J_f^\pi$	Feeding %
$^{86}\text{Se}$	704.3	$2_1^+ \rightarrow 0_1^+$	863.4	$4_1^+ \rightarrow 2_1^+$	90
			694.6	$2_2^+ \rightarrow 2_1^+$	10

TABLE II: continued...

Nuclei	Ground state	$J_i^\pi \rightarrow J_f^\pi$	Feeding	$J_i^\pi \rightarrow J_f^\pi$	Feeding
	transitions		transitions		%
	(keV)		(keV)		
$^{88}\text{Se}$	589.4	$2_1^+ \rightarrow 0_1^+$	961.9	$4_1^+ \rightarrow 2_1^+$	83
			653.5	$2_2^+ \rightarrow 2_1^+$	17
$^{88}\text{Kr}$	775.2	$2_1^+ \rightarrow 0_1^+$	868.4	$4_1^+ \rightarrow 2_1^+$	95
			802.1	$2_2^+ \rightarrow 2_1^+$	2
			1328.9	$4_2^+ \rightarrow 2_1^+$	3
$^{90}\text{Kr}$	707.0	$2_1^+ \rightarrow 0_1^+$	1123.4	$4_1^+ \rightarrow 2_1^+$	43
			1057.1	$\rightarrow 2_1^+$	23
			655.5	$2_2^+ \rightarrow 2_1^+$	34
$^{92}\text{Kr}$	768.8	$2_1^+ \rightarrow 0_1^+$	1035.3	$4_1^+ \rightarrow 2_1^+$	72
			1296.7	$4_2^+ \rightarrow 2_1^+$	28
$^{92}\text{Sr}$	814.9	$2_1^+ \rightarrow 0_1^+$	858.4	$4_1^+ \rightarrow 2_1^+$	81
			1370.0	$3_1^- \rightarrow 2_1^+$	19
$^{94}\text{Sr}$	836.9	$2_1^+ \rightarrow 0_1^+$	1309.1	$4_1^+ \rightarrow 2_1^+$	52
			1089.4	$3_1^- \rightarrow 2_1^+$	43
			1812.7	$4_2^+ \rightarrow 2_1^+$	5
$^{96}\text{Sr}$	815.0	$2_1^+ \rightarrow 0_1^+$	977.8	$4_1^+ \rightarrow 2_1^+$	64
			1160.6	$4_2^+ \rightarrow 2_1^+$	11
			692.0	$2_2^+ \rightarrow 2_1^+$	19
			1037.3	$3_1 \rightarrow 2_1^+$	6
$^{96}\text{Zr}$	1750.4	$2_1^+ \rightarrow 0_1^+$	1106.8	$4_1^+ \rightarrow 2_1^+$	32
			146.6	$3_1^- \rightarrow 2_1^+$	68
$^{98}\text{Zr}$	1222.9	$2_1^+ \rightarrow 0_1^+$	620.5	$4_1^+ \rightarrow 2_1^+$	66
			583.2	$3_1^- \rightarrow 2_1^+$	27
			1053.8	$4_3^+ \rightarrow 2_1^+$	4
			824.5	$4_2^+ \rightarrow 2_1^+$	2
			521.6	$2_3^+ \rightarrow 2_1^+$	1

TABLE II: continued...

Nuclei	Ground state	$J_i^\pi \rightarrow J_f^\pi$	Feeding	$J_i^\pi \rightarrow J_f^\pi$	Feeding
	transitions		transitions		%
	(keV)		(keV)		
$^{100}\text{Zr}$	212.5	$2_1^+ \rightarrow 0_1^+$	351.9	$4_1^+ \rightarrow 2_1^+$	97
			665.9	$2_2^+ \rightarrow 2_1^+$	2
			1185.4	$\rightarrow 2_1^+$	1
$^{102}\text{Zr}$	151.7	$2_1^+ \rightarrow 0_1^+$	326.4	$4_1^+ \rightarrow 2_1^+$	90
			1090.8	$3_1^+ \rightarrow 2_1^+$	10
$^{104}\text{Mo}$	192.2	$2_1^+ \rightarrow 0_1^+$	368.4	$4_1^+ \rightarrow 2_1^+$	84
			620.2	$2_2^+ \rightarrow 2_1^+$	4
			836.3	$3_1^+ \rightarrow 2_1^+$	12
$^{106}\text{Mo}$	171.5	$2_1^+ \rightarrow 0_1^+$	350.6	$4_1^+ \rightarrow 2_1^+$	81
			538.8	$2_2^+ \rightarrow 2_1^+$	8
			713.6	$3_1^+ \rightarrow 2_1^+$	11
$^{130}\text{Sn}^a$	1221.2	$2_1^+ \rightarrow 0_1^+$	774.3	$4_1^+ \rightarrow 2_1^+$	91
			807.0	$2_2^+ \rightarrow 2_1^+$	9
$^{132}\text{Sn}^a$	4041.1	$2_1^+ \rightarrow 0_1^+$	375.1	$4_1^+ \rightarrow 2_1^+$	98
			310.7	$3_1^- \rightarrow 2_1^+$	2
$^{132}\text{Te}^a$	974.0	$2_1^+ \rightarrow 0_1^+$	697.0	$4_1^+ \rightarrow 2_1^+$	98
			690.9	$2_2^+ \rightarrow 2_1^+$	2
$^{136}\text{Xe}^a$	1313.0	$2_1^+ \rightarrow 0_1^+$	381.3	$4_1^+ \rightarrow 2_1^+$	89
			976.5	$2_2^+ \rightarrow 2_1^+$	9
			812.6	$\rightarrow 2_1^+$	2
$^{138}\text{Xe}$	588.8	$2_1^+ \rightarrow 0_1^+$	483.7	$4_1^+ \rightarrow 2_1^+$	98
			875.2	$2_2^+ \rightarrow 2_1^+$	2
$^{140}\text{Xe}$	376.6	$2_1^+ \rightarrow 0_1^+$	457.6	$4_1^+ \rightarrow 2_1^+$	92
			927.9	$3_1^+ \rightarrow 2_1^+$	5
			1136.7	$3_1^- \rightarrow 2_1^+$	3
$^{144}\text{Ba}$	199.3	$2_1^+ \rightarrow 0_1^+$	330.8	$4_1^+ \rightarrow 2_1^+$	97

TABLE II: continued...

Nuclei	Ground state transitions (keV)	$J_i^\pi \rightarrow J_f^\pi$	Feeding transitions (keV)	$J_i^\pi \rightarrow J_f^\pi$	Feeding %
			638.9	$3_1^- \rightarrow 2_1^+$	3
$^{146}\text{Ba}$	181.0	$2_1^+ \rightarrow 0_1^+$	332.4	$4_1^+ \rightarrow 2_1^+$	91
			640.1	$3_1^- \rightarrow 2_1^+$	9
$^{144}\text{Ce}$	397.4	$2_1^+ \rightarrow 0_1^+$	541.2	$4_1^+ \rightarrow 2_1^+$	66
			844.8	$3_1^- \rightarrow 2_1^+$	34

<sup>a</sup> indicates that isomeric correction has been taken into account.

TABLE III: Third component of isospin ( $T_3$ ) and total isospin ( $T$ ) values of all the possible even-even fission fragments (FF) produced in the  $^{235}\text{U}(n_{th},f)$  reaction.

A	Nucleus	$T_3$	Nucleus	$T_3$	Nucleus	$T_3$	T
86	$^{86}\text{Se}$	9	$^{86}\text{Kr}$	7	$^{86}\text{Sr}$	5	9
88	$^{88}\text{Se}$	10	$^{88}\text{Kr}$	8	$^{88}\text{Sr}$	6	10
90	$^{90}\text{Kr}$	9	$^{90}\text{Sr}$	7	$^{90}\text{Zr}$	5	9
92	$^{92}\text{Kr}$	10	$^{92}\text{Sr}$	8	$^{92}\text{Zr}$	6	10
94	$^{94}\text{Kr}$	11	$^{94}\text{Sr}$	9	$^{94}\text{Zr}$	7	11
96	$^{96}\text{Sr}$	10	$^{96}\text{Zr}$	8	$^{96}\text{Mo}$	6	10
98	$^{98}\text{Sr}$	11	$^{98}\text{Zr}$	9	$^{98}\text{Mo}$	7	11
100	$^{100}\text{Sr}$	12	$^{100}\text{Zr}$	10	$^{100}\text{Mo}$	8	12
102	$^{102}\text{Zr}$	11	$^{102}\text{Mo}$	9	$^{100}\text{Ru}$	7	11
104	$^{104}\text{Zr}$	12	$^{104}\text{Mo}$	10	$^{104}\text{Ru}$	8	12
106	$^{106}\text{Mo}$	11	$^{106}\text{Ru}$	9	$^{106}\text{Pd}$	7	11
108	$^{108}\text{Mo}$	12	$^{108}\text{Ru}$	10	$^{108}\text{Pd}$	8	12
110	$^{110}\text{Mo}$	13	$^{110}\text{Ru}$	11	$^{110}\text{Pd}$	9	13
112	$^{112}\text{Ru}$	12	$^{112}\text{Cd}$	8	$^{112}\text{Pd}$	10	12
114	$^{114}\text{Ru}$	13	$^{114}\text{Cd}$	9	$^{114}\text{Pd}$	11	13
116	$^{116}\text{Ru}$	14	$^{116}\text{Cd}$	10	$^{116}\text{Pd}$	12	14

TABLE III: continued...

A	Nucleus	T <sub>3</sub>	Nucleus	T <sub>3</sub>	Nucleus	T <sub>3</sub>	T
118	<sup>118</sup> Sn	9	<sup>118</sup> Cd	11	<sup>118</sup> Pd	13	13
120	<sup>120</sup> Sn	10	<sup>120</sup> Cd	12	<sup>120</sup> Pd	14	14
122	<sup>122</sup> Te <sup>a</sup>	9	<sup>122</sup> Sn	11	<sup>122</sup> Cd	13	13
124	<sup>124</sup> Te	10	<sup>124</sup> Sn	12	<sup>124</sup> Cd	14	14
126	<sup>126</sup> Te	11	<sup>126</sup> Sn	13	<sup>126</sup> Cd	15	15
128	<sup>128</sup> Xe	10	<sup>128</sup> Te	12	<sup>128</sup> Sn	14	14
130	<sup>130</sup> Xe	11	<sup>130</sup> Te	13	<sup>130</sup> Sn	15	15
132	<sup>132</sup> Xe	12	<sup>132</sup> Te	14	<sup>132</sup> Sn	16	16
134	<sup>134</sup> Ba	11	<sup>134</sup> Xe	13	<sup>134</sup> Te	15	15
136	<sup>136</sup> Ba	12	<sup>136</sup> Xe	14	<sup>136</sup> Te	16	16
138	<sup>138</sup> Ba	13	<sup>138</sup> Xe	15	<sup>138</sup> Te	17	17
140	<sup>140</sup> Ce	12	<sup>140</sup> Ba	14	<sup>140</sup> Xe	16	16
142	<sup>142</sup> Ce	13	<sup>142</sup> Ba	15	<sup>142</sup> Xe	17	17

<sup>a</sup> indicates those nuclei which have been included for the sake of completeness of the table. However, the parameters corresponding to those nuclei do not affect the calculations, and have not been plotted in Fig. 7.

- 
- [1] J. H. Hamilton, A. V. Ramayya, S. J. Zhu, G. M. Ter-Akopian, Yu. Ts. Oganessian, J. D. Cole, J. O. Rasmussen and M. A. Stoyer, *Prog. Part. Nucl. Phys.* **35**, 635 (1995).
- [2] J. H. Hamilton *et al.*, *Prog. Part. Nucl. Phys.* **38**, 273 (1997).
- [3] J. H. Hamilton *et al.*, *Phys. Rep.* **264**, 215 (1996).
- [4] S. J. Zhu *et al.*, *Phys. Lett. B* **357**, 273 (1995).
- [5] D. C. Biswas *et al.*, *Eur. Phys. J* **A7**, 189 (2000).
- [6] D. C. Biswas *et al.*, *Phys. Rev. C* **71**, 011301 (2005).
- [7] W. Urban, J. L. Durell, A. G. Smith, W. R. Phillips, M. A. Jones, B. J. Varley, T. Rzaca-Urban, I. Ahmad, L. R. Morss, M. Bentaleb and N. Schulz, *Nucl. Phys. A* **689**, 605 (2001).
- [8] W. Urban *et al.*, *Z. Phys. A* **358**, 145 (1997).

- [9] M. Bentaleb, N. Schulz, E. Lubkiewicz, J. L. Durell, C. J. Pearson, W. R. Phillips, J. Shannon, B. J. Varley, I. Ahmad, C. J. Lister, L. R. Morss, K. L. Nash and C. W. Williams, *Z. Phys. A* **354**, 143 (1996).
- [10] A. Korgul, W. Urban, T. Rzaca-Urban, M. Rejmund, J. L. Durell, M. J. Leddy, M. A. Jones, W. R. Phillips, A. G. Smith, B. J. Varley, N. Schulz, M. Bentaleb, E. Lubkiewicz, I. Ahmad and L. R. Morss, *Eur. Phys. J. A* **7**, 167 (2000).
- [11] A. Bail, O. Serot, L. Mathieu, O. Litaize, T. Materna, U. Köster, H. Faust, A. Letourneau, and S. Panebianco, *Phys. Rev. C* **84**, 034605 (2011).
- [12] Y. K. Gupta *et al.*, *Phys. Rev. C* **96**, 014608 (2017).
- [13] S. Mukhopadhyay, L. S. Danu, D. C. Biswas, A. Goswami, P. N. Prashanth, L. A. Kinage, A. Chatterjee, and R. K. Choudhury, *Phys. Rev. C* **85**, 064321 (2012).
- [14] N. Fotiades, J. A. Cizewski, J. A. Becker, L. A. Bernstein, D. P. McNabb, W. Younes, R. M. Clark, P. Fallon, I. Y. Lee, A. O. Macchiavelli, A. Holt and M. Hjorth-Jensen, *Phys. Rev. C* **65** 044303 (2002).
- [15] D. Pantelica *et al.*, *Phys. Rev. C* **72**, 024304 (2005).
- [16] C. Y. Wu, H. Hua, D. Cline, A. B. Hayes, R. Teng, R. M. Clark, P. Fallon, A. Goergen, A. O. Macchiavelli and K. Vetter, *Phys. Rev. C* **70**, 064312 (2004).
- [17] L. S. Danu *et al.*, *Phys. Rev. C* **81**, 014311 (2010).
- [18] P. Banerjee, S. Ganguly, M. K. Pradhan, Md. Moin Shaikh, H. P. Sharma, S. Chakraborty, R. Palit, R. G. Pillay, V. Nanal, S. Saha, J. Sethi and D. C. Biswas, *Phys. Rev. C* **92**, 024318 (2015).
- [19] Japan Atomic Energy Agency : <https://www.ndc.jaea.go.jp/>.
- [20] D. C. Biswas, R. P. Vind, Nishant Kumar, Y. K. Gupta, R. V. Jangale, A. L. Inkar, L. A. Kinage, B. N. Joshi, S. Mukhopadhyay, G. K. Prajapati, Shradha Dubey, *Nucl. Instrum. Methods Phys. Res. A* **901**, 76 (2018).
- [21] W. Lang, H. G. Clerc, H. Wohlfarth, H. Schrader and K. H. Schmidt, *Nucl. Phys. A* **345**, 34 (1980).
- [22] P. Schillebeeckx, C. Wagemans, P. Geltenbort, F. Gönnenwein and A. Oed, *Nucl. Phys. A* **580**, 15 (1994).
- [23] R. B. Strittmatter, Thesis, University of Illinois (1978).
- [24] G. Rudstam, P. Aagaard, B. Ekström, E. Lund, H. Göktürk and H. U. Zwicky, *Radiochimica*

- Acta **49**, 155 (1990).
- [25] K. H. Schmidt, B. Jurado, C. Amouroux and C. Schmitt, Nucl. Data Sheets **131**, 107 (2016).
- [26] M. Jentschel *et al.*, JINST **12**, P11003 (2017).
- [27] G. de France, A. Blanc, F. Drouet, M. Jentschel, U. Köster, P. Mutti, J. M. Regis, G. Simpson, T. Soldner, O. Stezowski, S. Leoni, W. Urban and A. Vancrayenest, Pramana Journal of Physics **85**, 467 (2015).
- [28] P. Mutti, A. Blanc, G. de France, M. Jentschel, U. Köster, E. R. Martinez, G. Simpson, T. Soldner, C. A. Ur and W. Urban, Proc. ANNIMA Conf. (2013).
- [29] Radware : <http://radware.phy.ornl.gov/>.
- [30] D. C. Radford, Nucl. Instrum. Methods Phys. Res. A **361**, 297 (1995).
- [31] J. Theuerkauf, S. Esser, S. Krink, M. Luig, N. Nicolay, O. Stuch, and H. Wolters, <http://www.ikp.uni-koeln.de/~fitz/> (1993).
- [32] Evaluated Nuclear Structure Data File : <https://www.nndc.bnl.gov/ensdf>.
- [33] B. M. Musangu, A. H. Thibeault, T. H. Richards, E. H. Wang, J. H. Hamilton, C. J. Zachary, J. M. Eldridge, A. V. Ramayya, Y. X. Luo, J. O. Rasmussen, G. M. Ter-Akopian, Yu. Ts. Oganessian and S. J. Zhu, Phys. Rev. C **101**, 034610 (2020).
- [34] T. Kibédi, T. W. Burrows, M. B. Trzhaskovskaya, P. M. Davidson and C. W. Nestor, Nucl. Inst. and Meth. in Phys. Res. Sec. A **589**, 202 (2008).
- [35] J. N. Wilson *et al.*, PRL **118**, 222501 (2017).
- [36] D. Ramos *et al.*, PRL **123**, 092503 (2019).
- [37] H. Paşca, A. V. Andreev, G. G. Adamian, N. V. Antonenko, D. Lacroix, Phys. Rev. C **98**, 014624 (2018).
- [38] A. C. Wahl, At. Data Nucl. Data Tables **39**, 1 (1988).
- [39] A. M. Lane and J. M. Soper, Nucl. Phys. **37**, 663 (1962).
- [40] A. K. Jain, D. Choudhury and B. Maheshwari, Nucl. Data Sheet **120**, 123 (2014).
- [41] I. Kelson, Proc. of the Conference on Nuclear Isospin ed D Anderson *et al.*, 781 (1969).
- [42] S. Garg and A. K. Jain, Phys. Scr. **92**, 094001 (2017).
- [43] S. Garg, B. Maheshwari and A. K. Jain, Phys. Scr. **93**, 124008 (2018).
- [44] S. Garg and A. K. Jain, Pramana Journal of Physics **35**, 92 (2019).

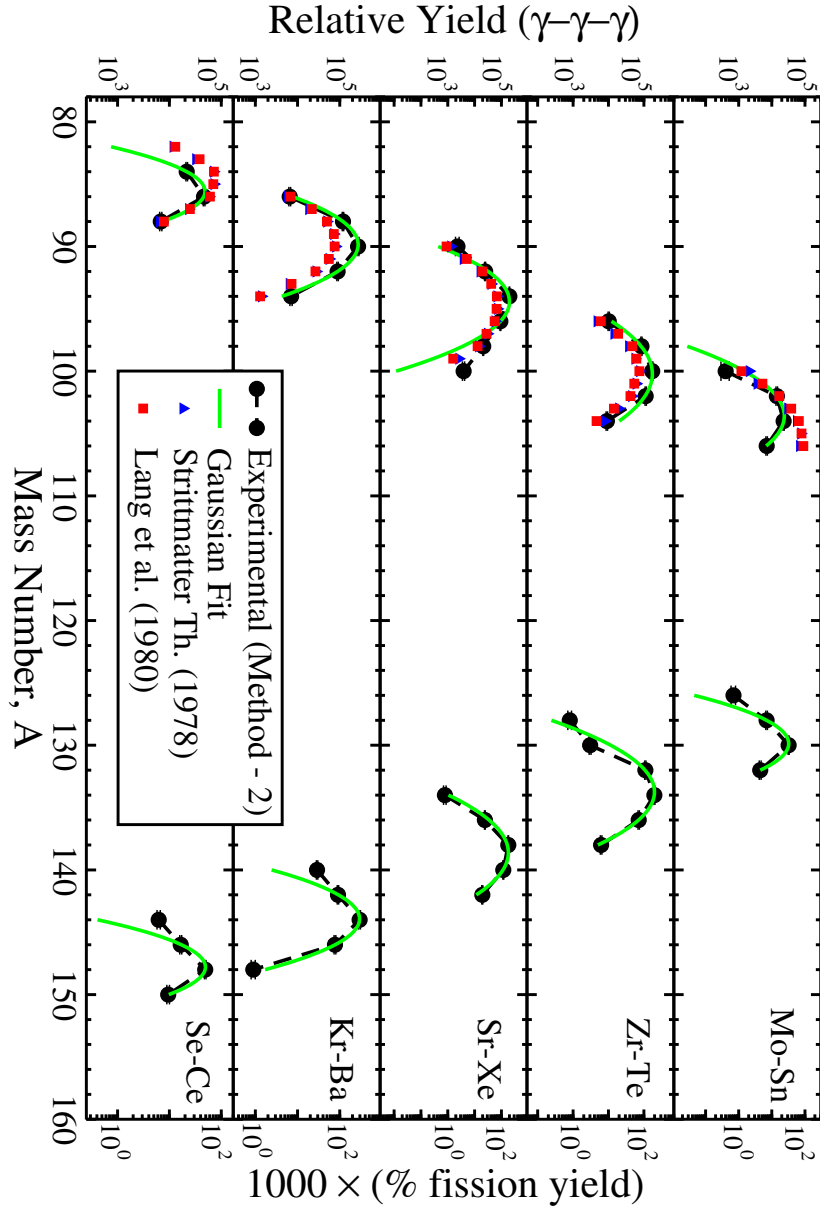


FIG. 6. (Color online) Comparison of the relative isotopic yield distribution of the complementary fission fragment nuclei obtained from the present investigation (by using the analysis procedure of Method-2) with those from the previous investigations. The Gaussian fit to the data has also been shown. Note the difference in the scale for the left and right ordinates. The scale of the left ordinate has been used for representing the relative yields extracted from the present gamma ray spectroscopic analysis. The right ordinate scale has been used for representing the yield data obtained from the previous measurements using recoil mass separators [21, 23]. See text for details.

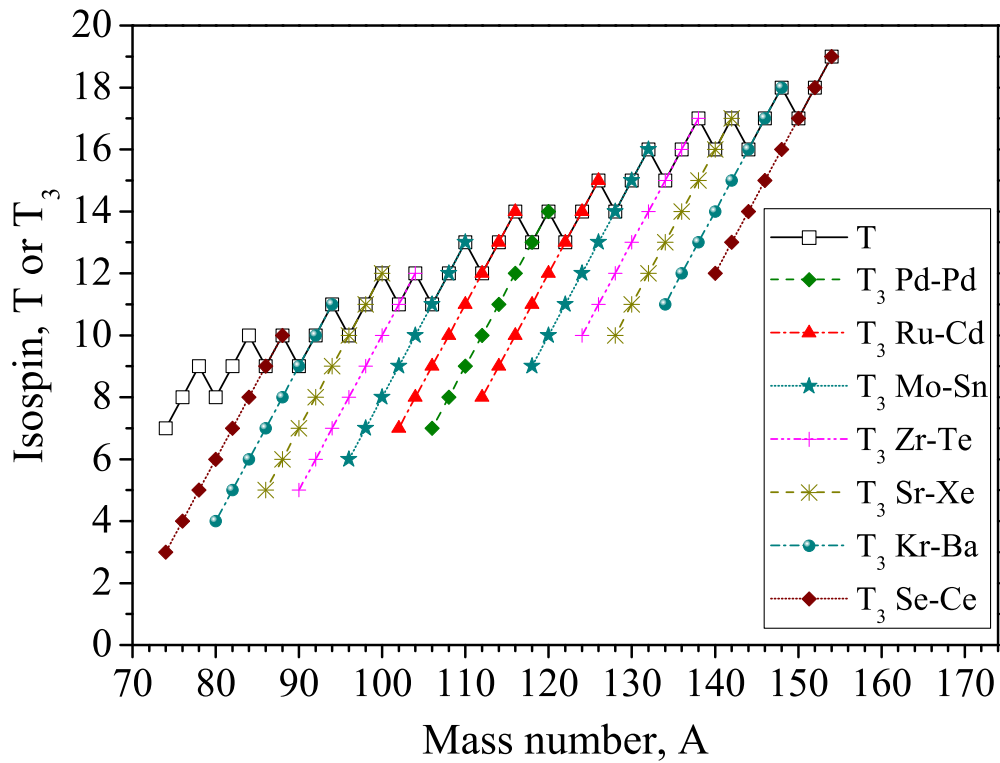


FIG. 7. (Color online) Depiction of isospin ( $T$  or  $T_3$ ) versus mass number ( $A$ ) for the fragment nuclei produced in the  $^{235}\text{U}(n_{th},f)$  reaction after neutron emissions. The open squares on the zig-zag line represent the isospin values ( $T$ ) that have been assigned to each mass number. The other symbols represent the  $T_3$  values for other fragment masses.